Dual-Channel Nonlinear Acquisition Circuit for High-Precision Wide-Range Temperature Control

Jiliang Qin, Zebo Zhang, Shi Qiao, Qixing Han, Xiaoli Jin, and Huadong Lu

***Abstract*—Temperature stability is paramount in precision engineering systems, but achieving high-precision temperature control over a wide temperature range remains challenging. To address this issue, this article proposes a temperature control system based on a dual-channel nonlinear acquisition circuit. The low-resolution (LR) channel and high-resolution (HR) channel are employed to achieve wide-range temperature monitoring and improve the sensitivity of temperature detection, respectively. After the dual-loop signal processing is coupled to the control system, the architecture achieves a temperature acquisition resolution of 0.00032 °C and a peak-to-peak value of temperature fluctuations below 0.006 °C ± 0.001 °C within 15 °C–75 °C during 1200 s. Compared to the traditional single-loop temperature control system, the temperature stability has been improved by an order of magnitude by employing the developed dual-loop temperature control system.**

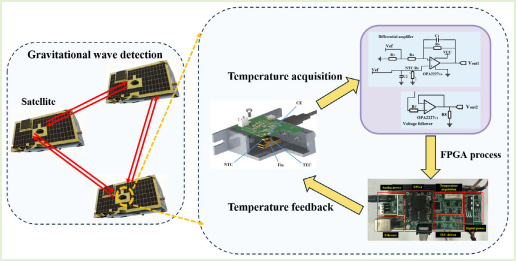

***Index Terms*— Dual-channel temperature acquisition, high precision, nonlinear amplification, wide range.**

I. Introduction

TEMPERATURE stability is a critical parameter in modern precision engineering systems [1], [2], including semiconductor manufacturing [3], [4] and biomedical instrumentations [5], [6], as well as space exploration equipment [7], [8]. In the extreme-precision measurement field, such as gravitational wave detection, thermal noise has emerged as a fundamental constraint on detection resolution [9]. In the advanced laser interferometer gravitational-wave observatory (Advanced LIGO) of the Max Planck Institute, if it is expected that the thermally induced optical path noise in optical platforms and thermal noise in the associated electronic/electrooptic systems are suppressed below the shot noise and the acceleration noise baseline, the temperature fluctuation spectral density has to be below 3 $\mathrm{mK}/\sqrt{\mathrm{Hz}}$ at 1×10^{-3} Hz [10]. These stringent requirements underscore the necessity of high-precision temperature control in the advanced detection systems. Especially in the weak light phase-locked system for gravitational wave detection, it requires high-temperature stability of the temperature-sensitive element and a low-temperature coupling coefficient, which forces the temperature control system to have high-temperature control accuracy in a relatively large temperature adjustment range. It is well known that a temperature control system usually comprises of three core modules, which are temperature measurements [11], [12], temperature-driven [13], [14], and control system [15], [16], [17], and the high-sensitive temperature acquisition in a wide temperature range is the key for achieving high-precision temperature control in a wide temperature range. However, an inherent tradeoff exists between measurement sensitivity and operational range, resulting in the inability to achieve high-precision temperature collection within a wide temperature range. To achieve wide-range control, in 2018, Shantanu Sarkar expanded the temperature control range covering −100 °C–100 °C by utilizing a multichannel high-precision temperature measurement system with resistance temperature detector and employing a single quartic function to address errors related to in-circuit resistance, tolerance, and temperature coefficient, but the accuracy was only ±0.02 °C [18]. Gao et al. [19] implemented a dual-sensor scheme within a dual-loop control framework—using an ADT7420 for coarse

Received 4 November 2025; revised 5 December 2025; accepted 12 December 2025. Date of publication 22 December 2025; date of current version 2 February 2026. This work was supported in part by the National Key Research and Development Program of China under Grant 2022YFC2204003. The associate editor coordinating the review of this article and approving it for publication was Prof. Jean-Michel Redoute. *(Jiliang Qin and Zebo Zhang contributed equally to this work.) (Corresponding author: Huadong Lu.)*

Jiliang Qin, Xiaoli Jin, and Huadong Lu are with the State Key Laboratory of Quantum Optics Technologies and Devices, Institute of Opto-Electronics, Shanxi University, Taiyuan 030006, China, and also with the Collaborative Innovation Center of Extreme Optics, Shanxi University, Taiyuan 030006, China (e-mail: luhuadong@sxu.edu.cn).

Zebo Zhang, Shi Qiao, and Qixing Han are with the State Key Laboratory of Quantum Optics Technologies and Devices, Institute of Opto-Electronics, Shanxi University, Taiyuan 030006, China.

Digital Object Identifier 10.1109/JSEN.2025.3645197

reference and a Pt100 for fine-tuning. This approach achieved a temperature range of −15 °C–50 °C with 0.5 °C accuracy. Yang et al. [20] proposed a proportional-divider resistance thermometer based on a voltage-reference design and achieved an accuracy better than 1 mK over the 10 °C–40 °C range. Jiang et al. [21] designed the temperature measurement system between the range of −35 °C–95 °C by employing a platinum resistance and self-heating effect measurement methods. However, the temperature measurement accuracy was only ±0.03 °C [21]. More recently, we have also introduced machine learning-based control methods into our temperature control systems. Although significant improvements in responsiveness and speed have been achieved, the temperature measurement accuracy remains limited [22], [23].

To overcome this limitation, here, we propose a dual-channel temperature acquisition system (DCTAS). This architecture comprises a coarse-resolution channel and a fine-resolution channel, where the former directly acquires real-time temperature values, while the latter specifically detects deviations between actual and setpoint temperatures. Critically, a preconfiguring circuit integrated into the fine-resolution channel enables programmable measurement range selection through tunable resistor settings. Coupled with differential amplification, this design achieves a substantial enhancement in temperature sensitivity, thereby overcoming the inherent constraints on acquisition resolution versus operational range to realize high-sensitivity monitoring across the extended temperature range. Experimental validation demonstrates that the proposed system attains a temperature resolution of 0.00032 °C within the 10 °C–80 °C range and maintains peak-to-peak steady-state fluctuations below 0.006 °C ± 0.001 °C within the 15°C–75 °C range. These results establish a viable pathway toward high-precision control across broad temperature range.

II. Experimental Design

To achieve the high-precision temperature control across a wide temperature range, a temperature control system based on the dual-channel temperature acquisition was designed and built, as shown in Fig. 1. The system architecture comprised three core modules, including a temperature acquisition module, a field-programmable gate array (FPGA) control module, and a thermoelectric cooler (TEC) driving module. Voltage signals from the NTC sensor were subsequently routed through dual amplification pathways: a low-sensitivity operational amplifier (OPA-LS) for wide-range monitoring and a high-sensitivity operational amplifier (OPA-HS) for high-sensitivity temperature detection. In the temperature acquisition module, a digital potentiometer (AD5143) controlled by the FPGA was used to configure tunable resistors (R_1, R_2), enabling automatic and dynamic adjustment of the high-sensitivity measurement center. Compared with the fixed-gain scheme, this strategy effectively overcame the limitations of insufficient sensitivity or local overamplification. Therefore, the temperature signals with a wide temperature range and local high sensitivity were successfully obtained. These signals

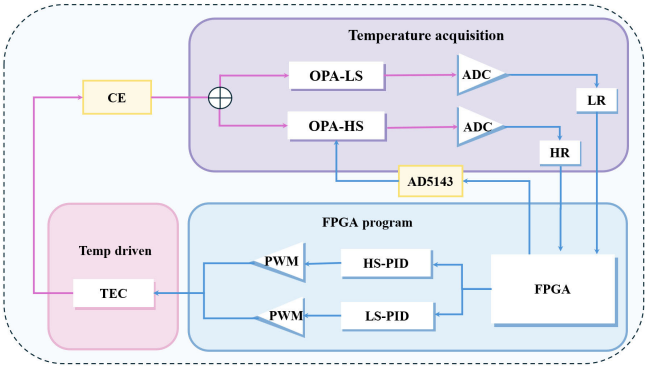

Fig. 1. Schematic of the designed temperature control system. The region of purple is the temperature acquisition part, the region of blue is the double-loops PID control part, and the region of pink is the TEC driven part. TEC: thermoelectric cooler; CE: controlled element.

were further digitized through analog-to-digital conversion (ADC) into low-resolution (LR) and high-resolution (HR) data streams and transmitted to the FPGA for the advanced processing. Within the FPGA, a dual-loop PID control algorithm processes data streamed to generate pulsewidth modulation (PWM) control signals with precise duty cycle. These control signals drove bidirectional TEC current regulators (heating/cooling modes), enabling real-time thermal stabilization of controlled elements (CEs) through closed-loop feedback.

To enable high-precision temperature control across extended operational ranges, HR acquisition over a wide temperature range constitutes a fundamental prerequisite. This requirement motivated the design of a dual-channel nonlinear acquisition circuit, as schematically depicted in Fig. 2. Crucially, to distinguish a submillikelvin temperature, a differential amplification circuit based on a high-precision low-noise operational amplifier OPA2227 is integrated into the acquisition architecture. In the circuit, the voltage of NTC (thermistor R_6) would be further processed through parallel pathways, including a voltage follower OPA2227_{U1} (low-sensitivity channel) and the differential amplifier OPA2227_{U0} (high-sensitivity channel). The voltage follower is used to monitor the temperature changes of NTC in the wide temperature range from −40 °C to 125 °C and the differential amplifier is mainly employed to distinguish the tiny temperature drift in a preset temperature range, and this preset temperature range is set based on the operating temperature range of the CE using the digital potentiometer R_2. Concurrently, to balance temperature sensitivity and the temperature range of local amplification, the gain K of the differential amplification circuit is about 200. To ensure the stability of gain with R_1 changes, the impedance of R_4 is required much larger than that of R_3 and R_1 in parallel.

According to Fig. 2, the output voltage V_{out2} of the low-sensitivity channel is $V_{\text{out2}} = V_{\text{ef}}/(1 + R_2/R_6)$. Here, V_{ef} is the constant reference voltage (5 V), $R_6(T) = R_0 e^{B(1/T-1/T_0)}$, T_0 is the reference temperature (25 °C), R_0 is the resistance (10 kΩ) of the thermistor at 25 °C, and B is the characteristic constant of the NTC thermistor (for a 10-kΩ thermistor and B is 3455). In the high-sensitivity

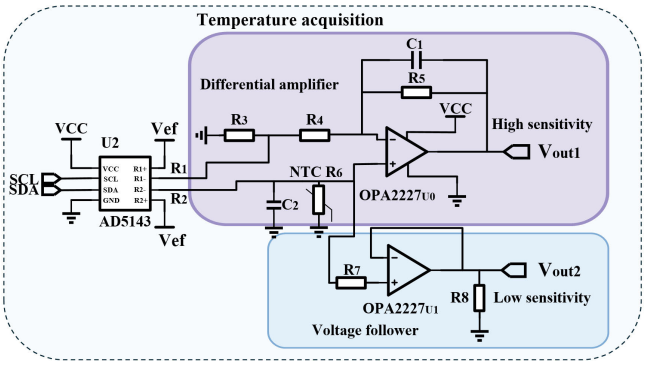

Fig. 2. Schematic of the temperature acquisition circuit. The purple region is high sensitive acquisition (V_{out1}) and the blue is low sensitive acquisition (V_{out2}). AD5143, digital potentiometer, there are R_1 and R_2 inside that can adjust the resistance value; OPA2227, operational amplifier; NTC, negative temperature coefficient sensor.

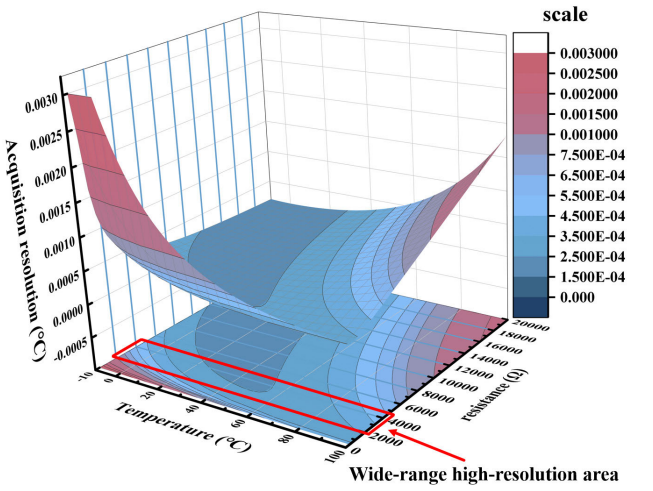

Fig. 3. 3-D graph of the temperature acquisition resolution of the HR channel with temperature and resistance R_2.

channel, when the temperature of NTC reaches the preset high-sensitivity temperature range, the output voltage $V_{out1} \approx (V_{out2} - V_{ef}/(1 + R_1/R_3))K$. When the NTC temperature is lower or higher than the preset temperature range, the output voltage V_{out1} is V_{oL} or V_{oH}, respectively. Thus, in the low-sensitivity channel, the relationship between output voltage V_{out2} and the temperature of the NTC can be expressed as the following equation:

$$T\left(V_{out2}\right) = \frac{B}{\ln\dfrac{V_{out2}\,R_2}{\left(V_{ef} - V_{out2}\right)\,R_0} + \dfrac{B}{T_0}}. \tag{1}$$

And in the high-sensitivity channel, the temperature $T(V_{out1})$ can be expressed as follows:

$$T\left(V_{out1}\right) = \frac{B}{\ln\dfrac{\left(V_{out1}/K + V_{ef}/\left(1 + R_1/R_3\right)\right)R_2}{\left(V_{ef}/\left(1 + R_3/R_1\right) - V_{out1}/K\right)R_0} + \dfrac{B}{T_0}}. \tag{2}$$

Here, $V_{oL} < V_{out1} < V_{oH}$, and the low-sensitivity temperature acquisition resolution ΔT_L is expressed as

$$\Delta T_L = \frac{\Delta V \cdot T^2 \cdot \left(R_0 e^{B\left(\frac{1}{T} - \frac{1}{T_0}\right)} + R_2\right)^2}{B \cdot V_{ef} \cdot R_2 \cdot e^{B\left(\frac{1}{T} - \frac{1}{T_0}\right)}} \tag{3}$$

where ΔV is the effective resolution voltage of the ADC (12 bits, AD9238), and the temperature acquisition resolution of the high-sensitive channel is $\Delta T_H = \Delta T_L/K$, which shows that the temperature acquisition resolution exhibits a functional dependence on both temperature T and resistor R_2.

To visualize this tripartite relationship explicitly, we present a 3-D graphical representation of their interdependencies in Fig. 3. According to Fig. 3, the acquisition resolution exhibits an extremum for different values of R_2, with corresponding variations in the temperature range and the resolution limit. In order to derive the resolution limit, (3) was differentiated with respect to T and the derivative was set to zero, leading to (4). Thus, (4) can be employed to determine the value of R_2 based on the required temperature acquisition range and the resolution requirements

$$R_2 = \frac{B - 2T}{B + 2T} R_0 e^{\left(\frac{1}{T} - \frac{1}{T_0}\right)}. \tag{4}$$

Once R_2 is determined, the value of R_1 is subsequently determined using (5), governed by the controlled temperature. The adjustment of R_1 can shift the high-sensitivity temperature measurement region

$$R_1 = \frac{R_2 \cdot R_3}{R_0 \cdot e^{B\left(\frac{1}{T} - \frac{1}{T_0}\right)}}. \tag{5}$$

As illustrated in Fig. 3, the temperature acquisition resolution is better than 0.0007 °C in the temperature of −10 °C–100 °C when the value of R_2 is approximately 2–4 kΩ. Therefore, in our experiment, a fixed value of 3 kΩ for R_2 is chosen and the resolution of the temperature acquisition is about 0.0003 °C. On this basis, the FPGA can automatically calculate the value of R_1 according to (5). Then, both R_1 and R_2 configure onto the circuit through the digital potentiometer AD5143 to complete the adaptive parameter deployment. Following this, the temperature sensitivities for the two channels were then calculated using (6) and (7), respectively

$$S_L = \frac{B \cdot V_{ef} \cdot R_2 \cdot e^{B\left(\frac{1}{T} - \frac{1}{T_0}\right)}}{T^2 \cdot \left(R_0 e^{B\left(\frac{1}{T} - \frac{1}{T_0}\right)} + R_2\right)^2} \tag{6}$$

$$S_H = \frac{K \cdot B \cdot V_{ef} \cdot R_2 \cdot e^{B\left(\frac{1}{T} - \frac{1}{T_0}\right)}}{T^2 \cdot \left(R_0 e^{B\left(\frac{1}{T} - \frac{1}{T_0}\right)} + R_2\right)^2}. \tag{7}$$

The sensitivity curves of the two channels are presented in Fig. 4. The blue curve corresponds to the low-sensitivity channel, while the red region represents the high-sensitivity channel. When the setpoint temperature changes, the resistor R_1 would be automatically adjusted by the control program, causing the high-sensitivity region to shift along the red dashed line.

In the control program, both HR and low-resolution temperature signal voltage values V_{out1} and V_{out2} are converted into digital data streams and transmitted to the FPGA for processing. In order to match the dual-channel signal acquisition architecture, a dual-path PID control algorithm is

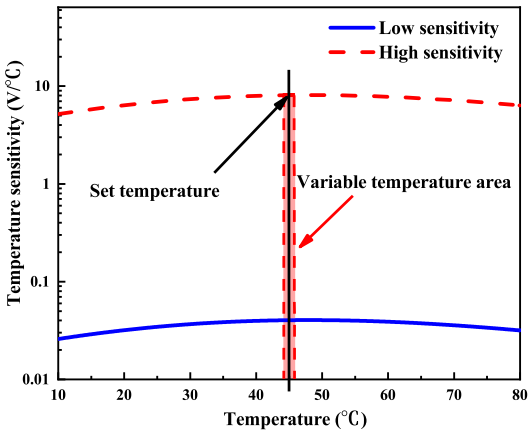

Fig. 4. Temperature sensitivity curves of the two channels.

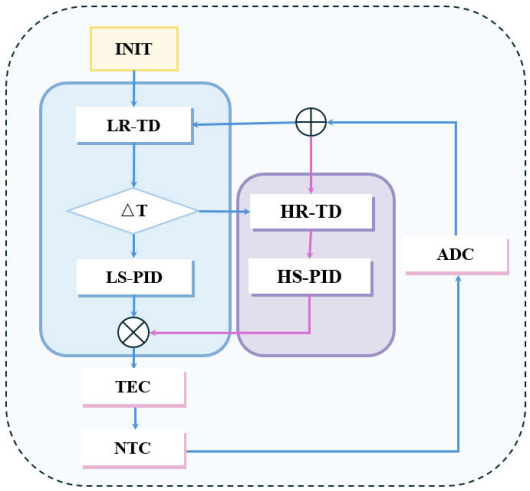

Fig. 5. Double loop PID control algorithm flowchart. The blue region is low-precision temperature control. The purple region is high-precision temperature control.

designed and the program flow diagram is illustrated in Fig. 5. In this program, the LR temperature data (LR-TD) enters the low-sensitivity PID (LS-PID) control algorithm channel, and the generated control signal is converted into the pulsewidth-modulated (PWM) signals to drive TEC (20031/035/020M) to achieve temperature control for CE. When the temperature reaches within ±0.01 °C of the setpoint, the system switches to the high-resolution PID (HS-PID) control mode by utilizing the HR temperature data (HR-TD). Thus, two closed loops are formed to realize multilevel precision control of temperature.

Following the completion of the circuit and control algorithm design, a rational structural design remains crucial for achieving the high-precision temperature control. The thermal interface is optimized by minimizing the distance between TEC and CE as much as possible to reduce the thermal loss and response delay. Surface-mounted NTC sensor is directly soldered onto a thermal pad to enhance the temperature acquisition speed and resolution. Furthermore, the compact structural design effectively mitigates the environmental interference, and the cross-sectional view of the implemented device structure is shown in Fig. 6, which includes the integrated temperature acquisition and driving modules.

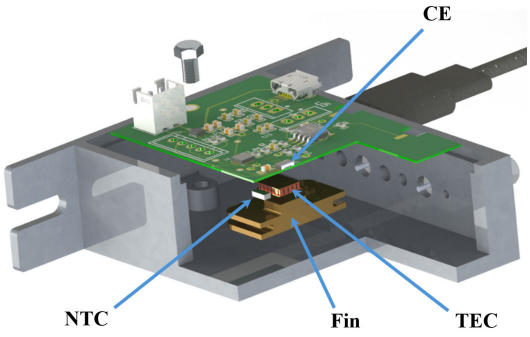

Fig. 6. Physical structure of the temperature control system. Fin, heat sink.

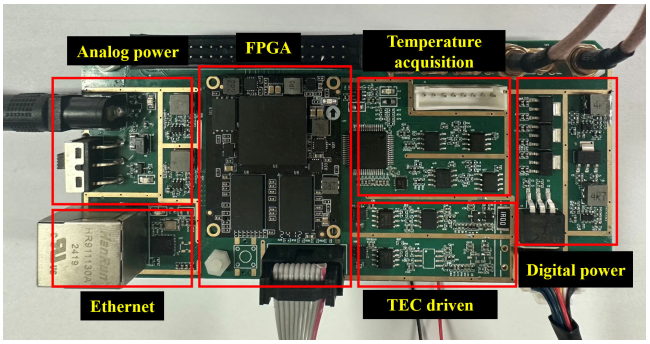

Fig. 7. PCB hardware circuit structure of the temperature control system. The PCB size is 140 × 65 mm.

The overall hardware architecture of the temperature control system is depicted in Fig. 7. The architecture incorporates five fundamental modules integrated compactly on a four-layer printed circuit board (PCB): a temperature acquisition module, an FPGA control module, a TEC driver module, isolated analog and digital power supply modules, and an Ethernet communication module. The temperature acquisition module is implemented based on the circuit schematic in Fig. 2. The FPGA control module is built around a Xilinx Zynq-7020 and supplemented with DDR4 memory, flash storage, and clock generation circuitry. The TEC driver employs a dedicated driver IC (DRV8212DSGR), whose output port is connected to the TEC element through external cables. To mitigate digital noise coupling into analog signals, the analog and digital power supplies are strictly isolated, emphasizing the separation of the analog ground (AGND) and digital ground (DGND) planes. Finally, the Ethernet module serves as the primary communication interface for external monitoring and control, enabling real-time adjustment of system parameters and retrieval of operational status.

To guarantee reliable temperature measurement with the developed control system, the measurement noise must be assessed. The primary sources of noise in the temperature acquisition system include amplifier noise, resistor thermal noise, and ADC quantization noise. Notably, in our system, the ADC sampling rate is set to 10 kSPS. However, due to the slow thermal response, the temperature signal is filtered by a digital filter with a bandwidth of $B = 10$ Hz, which sets the effective noise bandwidth. Specifically, the equivalent input

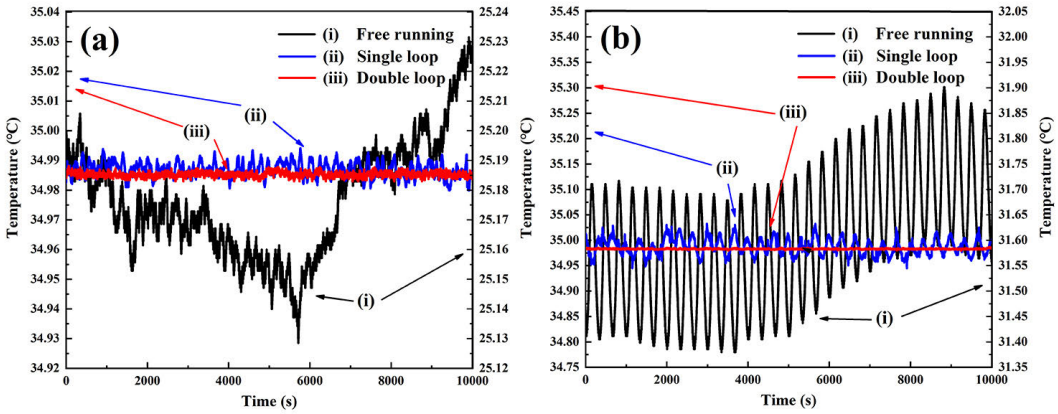

Fig. 8. Measured temperature fluctuations in 10 000 s. (a) and (b) Represent the results for power on and periodic conversion.

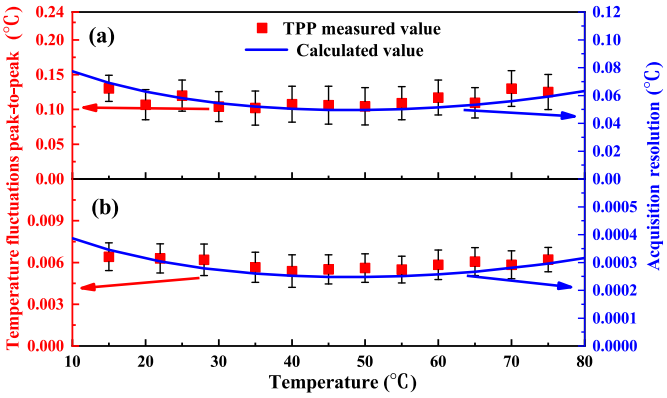

Fig. 9. Temperature acquisition resolution and peak-to-peak value of temperature control fluctuation for (a) single loop and (b) double loop. The red dots represent the temperature fluctuations of peak-to-peak (TPP), and the blue curve represents the calculated acquisition resolution.

voltage rms noise (V_{rms}) of the low-noise amplifier OPA2227 is 15 nV (1–10 Hz), the resistor thermal noise is given by $(4kTR_4B)^{1/2}$, and the quantization noise N_q is 0.289 least significant bit (LSB). The total noise can thus be expressed by the following equation:

$$N_{\text{sum}} \approx \sqrt{(V_{\text{rms}}K)^2 + 4kTR_4B\left(K^2 + K\right) + \left(N_q\right)^2}. \quad (8)$$

Substituting the circuit parameters into this formula, it can be calculated that N_{sum} is approximately 0.35 mV, which is less than $\Delta V = 1.2$ mV. Therefore, the temperature acquisition system achieves a relatively high degree of accuracy.

III. Experimental Results

In order to test the performance of the developed temperature control system, an integrated circuit chip (DAC, B9122) was employed as the CE in the experiment. When CE is only power ON, its thermal power dissipation was relatively low. The temperature fluctuation of peak-to-peak (TPP) for free-running depicted in curve 1) of Fig. 8(a) and the responding standard deviation (STD) were 0.10298 °C in 10 000 s and 0.01907 °C, respectively, when the ambient temperature was 25 °C. At this time, the TPP in 10 000 s was reduced to 0.01435 °C and 0.00515 °C when the traditional single-loop control circuit (only a temperature acquisition and a PID control program) and our designed dual-loop control circuit were employed to control the temperature of CE to 35 °C, respectively, which were shown in curve 2) and curve 3) of Fig. 8(a). The STD was reduced to 0.00249 °C and 0.00070 °C, respectively. On this basis, a periodic conversion rate was loaded on the CE, and a periodic temperature fluctuation was easily observed in experiment, as shown in curve 1) of Fig. 8(b). It was clear that the average temperature of the CE increased to 31.7 °C for the free-running and the TPP in 10 000 s was as high as 0.52178 °C with the oscillation periodic of 333 s. The responding STD was also higher than 0.12948 °C. In this case, the TPP and responding STD were reduced to 0.08749 °C and 0.01602 °C, respectively, when the traditional single-loop control circuit was used in experiment. However, once our designed dual-loop control circuit was employed, the TPP and the responding STD were effectively to as small as 0.00732 °C and 0.00065 °C, respectively. Therefore, compared with the traditional single-loop control, the dual-loop control based on dual-channel temperature acquisition improved STD stability by approximately 25×. All data were listed into Table I. The measured results revealed the inherent limitation of the single-loop architectures constrained by its temperature acquisition resolution, and it was well concluded that the developed dual-loop system reduced both fluctuation metrics by over one order of magnitude and achieved submillikelvin stability essential for the precision metrological applications.

TABLE I
Temperature Measurement Results

Experiment	power on		periodic conversion	
	TPP	STD	TPP	STD
Free running	0.10298°C	0.01907°C	0.52178°C	0.12948°C
Single loop	0.01435°C	0.00249°C	0.08749°C	0.01602°C
Double loop	0.00515°C	0.00070°C	0.00732°C	0.00065°C

At last, the performances of the single-loop and dual-loop control systems in a wide temperature range from 15 °C to 75 °C were further evaluated by configuring R_2 at 3 kΩ. Based on (2) and the ΔT_H, the temperature acquisition resolutions

TABLE II
TEMPERATURE RANGE AND PRECISION COMPARISON

Method	Temperature Range (°C)	accuracy (°C)	Reference
Multi-point calib.	−100˜100	±0.02	[18]
Dual-sensor fusion	−15˜50	≈ 0.5	[19]
Ratiometric divider meas.	10˜40	< 0.001	[20]
Self-heating	−35˜95	±0.03	[21]
DCTAS	10˜80	≤0.00032	This work

of single loop and double loop versus the temperature were plotted as the blue curve in Fig. 9(a) and 9(b). It was seen that the calculated minimum acquisition resolution was as low as 0.00025 °C at the temperature of 45 °C, and this acquisition resolution could slightly decreased when the temperature was away from 45 °C. At the same time, the measurements of temperature fluctuations across 15 °C–75 °C range were conducted with 1200-s measurement duration and five repeated measurements per temperature point and the TPP values of measurement data at each setpoint are marked as red points in Fig. 9(b). The experimental results demonstrated that the dual-channel acquisition circuit maintains high-temperature resolution (≤0.00032 °C) throughout 10 °C–80 °C range, achieving optimal resolution of 0.00025 °C at 45 °C when $R_2 = 3$ kΩ. Concurrently, the control system exhibits superior stability across this temperature range, with a TPP of 0.006 °C ± 0.001 °C. This is significantly superior to the single-loop control with a TPP of 0.11 °C ± 0.02 °C.

A direct comparison with previous studies, provided in Table II, confirms that our DCTAS achieves a superior combination of temperature range and sensitivity, making its advancement readily apparent.

IV. CONCLUSION

In a word, this study presented a dual-loop temperature control system, which resolved the inherent tradeoff between the high resolution and wide-range acquisition in the precise temperature control. By configurating the values of R_2 and R_1 to implement the balance between the resolution and range as well as the dynamic temperature setting, respectively, a nonlinear amplification dual-channel temperature acquisition circuit with the adaptive parameter optimization was structured. As a result, we achieved the HR acquisition (0.00025 °C resolution at 45 °C) in the wide temperature range (10 °C–80 °C). Then, in order to achieve high-precision temperature control with the DCTAS, we developed a double-loop PID program based on FPGA to obtain the feedback control signal. The control signal regulated the temperature of the controlled component through the high-precision TEC temperature drive module to achieve high-precision temperature control, and TPP and standard deviation STD were effectively reduced to 0.007 °C–0.00065 °C from 0.52 °C to 0.12948 °C for the uncontrolled chip within 10 000 s, respectively. At last, in the temperature range of 15 °C–75 °C, the TPP is mostly less than 0.006 °C ± 0.001 °C within 1200 s. The experimental validation demonstrated remarkable performance enhancements. We believe that this work establishes a hardware–software co-design paradigm for ultraprecision temperature control across broad temperature operational ranges and the achieved temperature control system can meet stringent requirements for special applications, such as gravitational wave detection.

REFERENCES

[1] M. Xu and C. Chen, "Application and research of intelligent temperature control system based on deep learning in precision manufacturing product design," *Thermal Sci. Eng. Prog.*, vol. 57, Jan. 2025, Art. no. 103185.

[2] Q. Sun et al., "Design and development of laser temperature control system of LHAASO," *J. Instrum.*, vol. 18, no. 6, Jun. 2023, Art. no. T06008.

[3] Y. Zhao, Z. Tian, X. Feng, Z. Feng, X. Zhu, and Y. Zhou, "High-precision semiconductor laser current drive and temperature control system design," *Sensors*, vol. 22, no. 24, p. 9989, Dec. 2022.

[4] Z. Li et al., "Design and performance test of the spaceborne laser in the TianQin-1 mission," *Opt. Laser Technol.*, vol. 141, Sep. 2021, Art. no. 107155.

[5] Y. Zhu, L. Ke, Y. Wei, and X. Zheng, "A high-precision real-time temperature acquisition method based on magnetic nanoparticles," *Sensors*, vol. 24, no. 23, p. 7716, Dec. 2024.

[6] Z. E. Jeroish, K. S. Bhuvaneshwari, F. Samsuri, and V. Narayanamurthy, "Microheater: Material, design, fabrication, temperature control, and applications-A role in COVID-19," *Biomed. Microdevices*, vol. 24, no. 1, Dec. 2021, Art. no. 3.

[7] X. Zhang, H. Liang, J. Feng, and H. Tan, "Kalman filter based high precision temperature data processing method," *Frontiers Energy Res.*, vol. 10, Apr. 2022, Art. no. 832346.

[8] H. Hu, S. Chang, Y. Li, and X. Li, "Design and thermal characteristic test of a temperature control system for spacecraft precision instrument," *Int. J. Refrig.*, vol. 146, pp. 462–470, Feb. 2023.

[9] H. Dong, W. Zhang, M. Li, Z. Zeng, D. Cao, and X. Li, "High-precision air temperature control considering both hardware elements and controller design," *Case Stud. Thermal Eng.*, vol. 37, Sep. 2022, Art. no. 102290.

[10] S. Barke, Y. Wang, J. J. E. Delgado, M. Tröbs, G. Heinzel, and K. Danzmann, "Towards a gravitational wave observatory designer: Sensitivity limits of spaceborne detectors," *Classical Quantum Gravity*, vol. 32, no. 9, Apr. 2015, Art. no. 095004.

[11] C. Goumopoulos, "A high precision, wireless temperature measurement system for pervasive computing applications," *Sensors*, vol. 18, no. 10, p. 3445, Oct. 2018.

[12] S. Ma et al., "Optical fiber sensors for high-temperature monitoring: A review," *Sensors*, vol. 22, no. 15, p. 5722, Jul. 2022.

[13] X. Xu, J. Zhang, and X. Wang, "Multi-channel precision temperature control system based on TEC," in *Proc. IEEE Int. Conf. Mechatronics Autom. (ICMA)*, Oct. 2020, pp. 1992–1997.

[14] S. He et al., "A 120 °C operating range TEC-less uncooled IRFPA with on-chip real-time ultralow temperature drift compensation," *IEEE Sensors J.*, vol. 25, no. 12, pp. 22641–22651, Jun. 2025.

[15] X. Song et al., "An integrated gold-film temperature sensor for in situ temperature measurement of a high-precision MEMS accelerometer," *Sensors*, vol. 20, no. 13, p. 3652, Jun. 2020.

[16] X. Li, Z. Wang, W. Chen, X. Ning, W. Quan, and Y. Zhai, "Double-loop control and intelligent parameter tuning for the temperature control system of a DBR semiconductor laser," *Appl. Opt.*, vol. 60, no. 2, p. 326, 2021.

[17] F.-S. Lin, M.-C. Huang, S.-K. Tai, Y.-C. Chu, S.-H. Shen, and C.-H. Huang, "Investigation of an FPGA-based acoustic gas thermometer for monitoring indoor temperature distribution two-dimensionally," *IEEE Sensors J.*, vol. 24, no. 9, pp. 15197–15209, May 2024.

[18] S. Sarkar, "Platinum RTD sensor based multi-channel high-precision temperature measurement system for temperature range −100°C to +100°C using single quartic function," *Cogent Eng.*, vol. 5, no. 1, Jan. 2018, Art. no. 1558687.

[19] X. Gao, Q. Ma, X. Sun, J. Wang, and S. Li, "Research on a dual-closed-loop temperature control method and system based on dual sensors for infrared object simulation," *IEEE Sensors J.*, vol. 19, no. 23, pp. 11553–11561, Dec. 2019.

[20] H. Yang, R. Yang, X. Wang, Z. Yin, P. Hu, and J. Tan, "Design of a high-precision, high environmental adaptability temperature measurement system for environments with large temperature variations," *AIP Adv.*, vol. 12, no. 11, Nov. 2022, Art. no. 115214.

[21] L. Jiang, C. Liu, L. Zhu, Z. Zhang, and Q. Hou, "High-precision and wide-range temperature measurement and control system of satellite-borne calibration blackbody," *Measurement*, vol. 231, May 2024, Art. no. 114591.

[22] H. Qiao, W. Peng, P. Jin, J. Su, and H. Lu, "Performance improvement of single-frequency CW laser using a temperature controller based on machine learning," *Micromachines*, vol. 13, no. 7, p. 1047, Jun. 2022.

[23] Y. He, X. Jin, P. Jin, J. Su, F. Li, and H. Lu, "Temperature control performance improvement of high-power laser diode with assistance of machine learning," *Photonics*, vol. 12, no. 3, p. 241, Mar. 2025.

Jiliang Qin was born in Chongqing, China, in 1990. He received the Ph.D. degree in optics from the Institute of Opto-Electronics, Shanxi University, Taiyuan, China, in 2019.

He is currently a Lecturer with the Institute of Opto-Electronics, Shanxi University. His current research interests include solid-state laser technology, optoelectronic technology, and quantum optics.

Zebo Zhang was born in Shanxi, China, in 2001. He received the B.E. degree in mechanical design from Taiyuan Institute of Technology, Taiyuan, China, in 2023. He is currently pursuing the master's degree in optoelectronic information engineering with the School of Physics and Electronic Engineering, Shanxi University, Taiyuan.

His research interests include optoelectronic detection technology and embedded systems.

Shi Qiao was born in Shanxi, China, in 1998. He received the B.E. degree in electrical engineering and intelligent control from North University of China, Taiyuan, China, in 2020. He is currently pursuing the master's degree in optoelectronic information engineering with the School of Physics and Electronic Engineering, Shanxi University, Taiyuan.

His research interests include optoelectronic detection technology and artificial intelligence.

Qixing Han was born in Shanxi, China, in 2000. He received the B.E. degree in automation from Jilin Agricultural University, Changchun, China, in 2023. He is currently pursuing the master's degree in optoelectronic information engineering with the School of Physics and Electronic Engineering, Shanxi University, Taiyuan, China.

His research interests include optoelectronic detection technology and artificial intelligence.

Xiaoli Jin was born in Shanxi, China, in 1984. She received the Ph.D. degree in optics from the Institute of Opto-Electronics, Shanxi University, Taiyuan, China, in 2016.

She is currently an Associate Professor with the Institute of Opto-Electronics, Shanxi University. Her current research interests include the design and control of driver for solid-state laser, optoelectronic detection technology, and machine learning.

Huadong Lu was born in Shanxi, China, in 1981. He received the Ph.D. degree in laser technology from Shanxi University, Taiyuan, China, in 2011.

He is currently a Professor with the Institute of Optoelectronics, Shanxi University. His current research interests include all-solid-state laser technology, quantum optics devices, and tunable optics devices.